Thermal Decomposition Kinetics of Glyphosate (GP) and its Metabolite Aminomethylphosphonic Acid (AMPA)

Milad Narimani,[a] Gabriel da Silva[a,]*

[a]Department of Chemical Engineering, University of Melbourne, Victoria 3010, Australia.

*Corresponding author. Email: gdasilva@unimelb.edu.au

Abstract

Glyphosate (GP) is a widely used herbicide worldwide, yet accumulation of GP and its main byproduct, aminomethylphosphonic acid (AMPA), in soil and water has raised concerns about its potential effects to human health. Thermal treatment processes are one option for decontaminating material containing GP and AMPA, yet the thermal decomposition chemistry of these compounds remains poorly understood. Here, we have revealed the thermal decomposition mechanism of GP and AMPA by applying computational chemistry and reaction rate theory methods. The preferred decomposition channel for both substances involves the elimination of $P(OH)_3$ to yield the imine *N*-methylene-glycine (from GP) or methanimine (from AMPA), with relatively low barrier heights (*ca*. 45 kcal/mol). The half-life of GP and AMPA at 1000 K are predicted to be 0.1 and 4 ms respectively, and they should be readily destroyed via conventional incineration processes. The further decomposition of *N*-methylene-glycine is expected to also take place at similar temperatures, leading to *N*-methyl-methanimine + CO_2, with a barrier height of ca. 48 kcal/mol. The imine decomposition products of GP and AMPA are also expected to undergo hydrolysis to simple amines and carbonyl compounds.

Keywords

Glyphosate, Aminomethylphosphonic Acid, AMPA, Thermal decomposition, Incineration, Density functional theory, Transition state theory

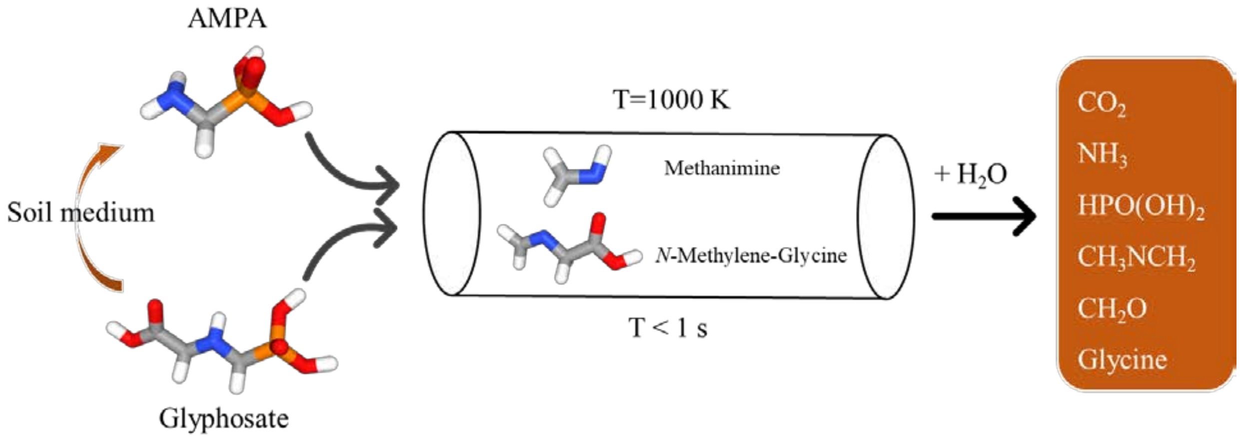

INTRODUCTION

Glyphosate (GP), *N*-(phosphonomethyl) glycine, is a non-selective, systematic, and post emergent herbicide capable of controlling more weed species than other herbicides.[1-3] The introduction of glyphosate-resistant crops in 1996 further amplified its importance.[3] The widespread use of GP has resulted in its accumulation in soil and water.[4-7] The microbial degradation of GP in soil, natural waters and plants, or metabolization by select plant species, can lead to the formation of aminomethylphosphonic acid (AMPA); AMPA is more toxic and persistent than GP.[8-12] In addition to GP, a number of other phosphonate compounds, including detergents, can degrade to AMPA.[13, 14] The structures of GP and AMPA are shown in Fig. 1.

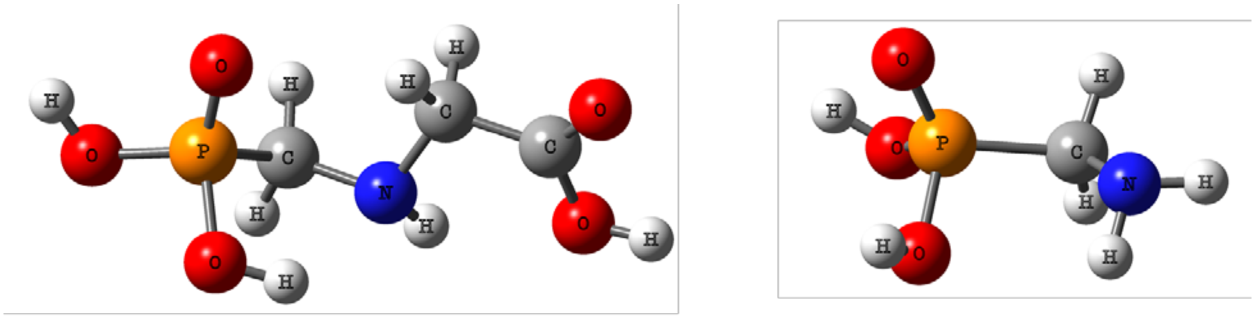

(a) (b)

Fig. 1 Structure of (a) glyphosate (GP) and (b) aminomethylphosphonic acid (AMPA).

There are major concerns about residual GP and its major metabolite AMPA in aquatic and terrestrial environments. Numerous studies have demonstrated that GP has mutagenic and carcinogenic effects [15], genotoxic effects [16], and endocrinal effects [17] on humans. As a result the World Health Organization (WHO) declared this herbicide to be carcinogenic to humans in 2015 [18].

Several treatment processes have been developed to remove pesticide contamination from soil and water. These remediation technologies can be classified into physical, biological and chemical processes [19]. Physical treatment processes, including adsorption [20, 21], and filtration methods [22, 23], produce concentrated waste streams that require post-treatment processing in order to be converted to non-toxic products. Although bioremediation technologies can destroy the target contaminants, the main obstacle to their applicability is long residence times.[24] Chemical remediation processes are under development to remove GP from wastewater.[25-27] The major concern with chemical remediation is the need for further treatment of degradation products, which can have worse effects than their parent pesticides.[19, 20]

Thermal treatment methods including incineration and pyrolysis are well-established destruction strategies for solid waste management. The main advantages of thermochemical treatment processes are waste volume reduction, toxic compound destruction, and residual energy recovery.[28] In order to develop and optimize thermal treatment processes for the destruction of GP and AMPA we require a fundamental understanding of their decomposition chemistry, particularly the products formed and temperature-dependent reaction rates. A wide variety of organophosphates are encountered in thermal systems, and insights into GP and AMPA decomposition will also aid in the development of broader chemical kinetic models for organophosphate combustion and pyrolysis.[29-34]

In this work, the detailed decomposition mechanism and kinetics of GP and AMPA are presented for the first time using computational chemistry and statistical reaction rate theory techniques. This study identifies the most probable products of the initial stages of the GP and AMPA decomposition mechanisms and their corresponding rate coefficients as a function of temperature.

METHODS

Quantum chemistry calculations were conducted in Gaussian 16.[35] Geometry optimizations, frequency calculations, and intrinsic reaction coordinate (IRC) calculations were carried out at the M06-2X/6-31G(2df,p) level of theory. Subsequently, the equilibrium structures were utilized in high-level composite G3X-K energy calculations.[36] The structural coordinates, vibrational frequencies, and electronic energies of reactants and transition states were then used in Multiwell-2016 program suit [37, 38] to calculate rate coefficients using canonical transition state theory. Rate coefficients of all identified reaction channels were calculated in the temperature range of 300-2000 K for both GP and AMPA.

RESULTS AND DISCUSSION

GP Decomposition

The lowest-energy reaction channels identified for the isomerization and decomposition of GP are demonstrated in Fig. 2. The process with the lowest barrier height corresponds to simultaneous C—P bond cleavage and proton transfer from the nitrogen to the P=O oxygen atom. This pathway requires 44.9 kcal/mol and leads to formation of $P(OH)_3$ and *N*-methylene-glycine via **TS1G** (Fig. 3a). There is little available experimental information on the thermal decomposition of GP, although a calorimetric study identified that the first stage of decomposition proceeds with an activation energy of 48.1 kcal/mol [39], in relative agreement with our calculations. Moreover, this step was found to be endothermic and to likely result in loss of a methylene group in GP, again consistent with our proposed mechanism.

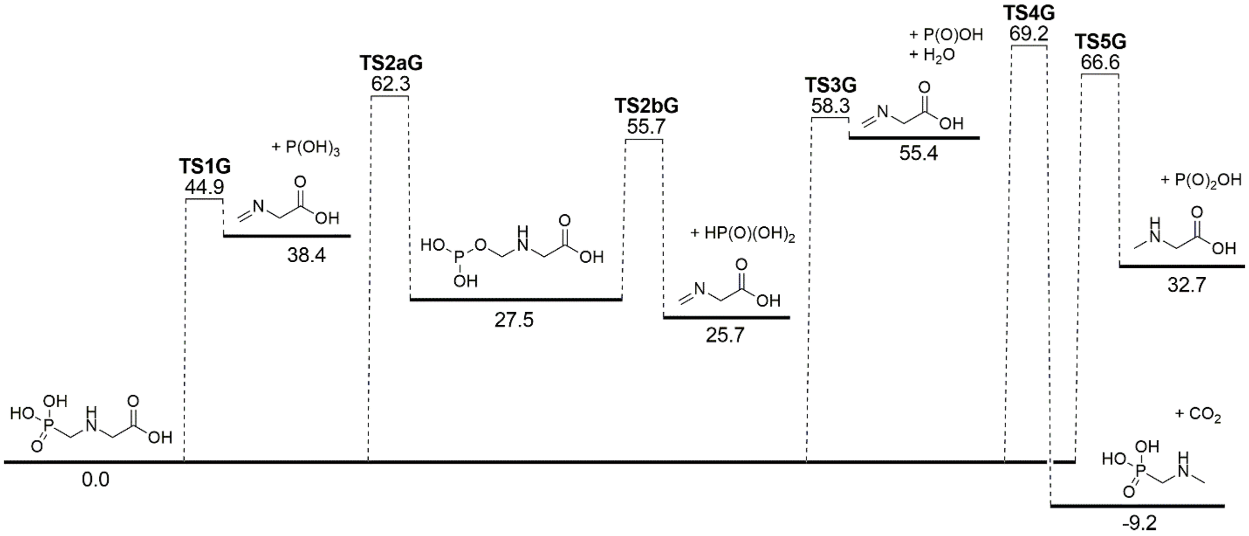

Fig. 2 Potential energy diagram for the thermal decomposition of GP. Energies (0 K enthalpies) are calculated at the G3X-K level of theory.

Several higher-energy decomposition pathways are also identified in GP decomposition, and are included in Fig. 2. Pathway 2 (**TS2aG**, **TS2bG**) also leads to *N*-methylene-glycine formation, but with phosphoric acid ($HP(O)(OH)_2$) as the co-product. Although $HP(O)(OH)_2$ is more stable than $P(OH)_3$, the higher barriers along pathway 2 mean that this pathway is unlikely to be favored. However, subsequent to the formation of $P(OH)_3$ it is likely to rearrange to $HP(O)(OH)_2$, where the barrier height is calculated to be 49.4 kcal/mol at the G3X-K level of theory. Pathway 3 demonstrates how water elimination can also lead to the production of *N*-methylene-glycine, along with P(O)OH, with a relatively large barrier height of 58.3 kcal/mol. Finally, pathways 4 and 5 lead to amine formation via elimination of the carboxylate (**TS4G**) or phosphate (**TS5G**) groups, respectively. Both reactions have similar barrier heights at ca. 70 kcal/mol, and are unexpected to compete with pathway 1.

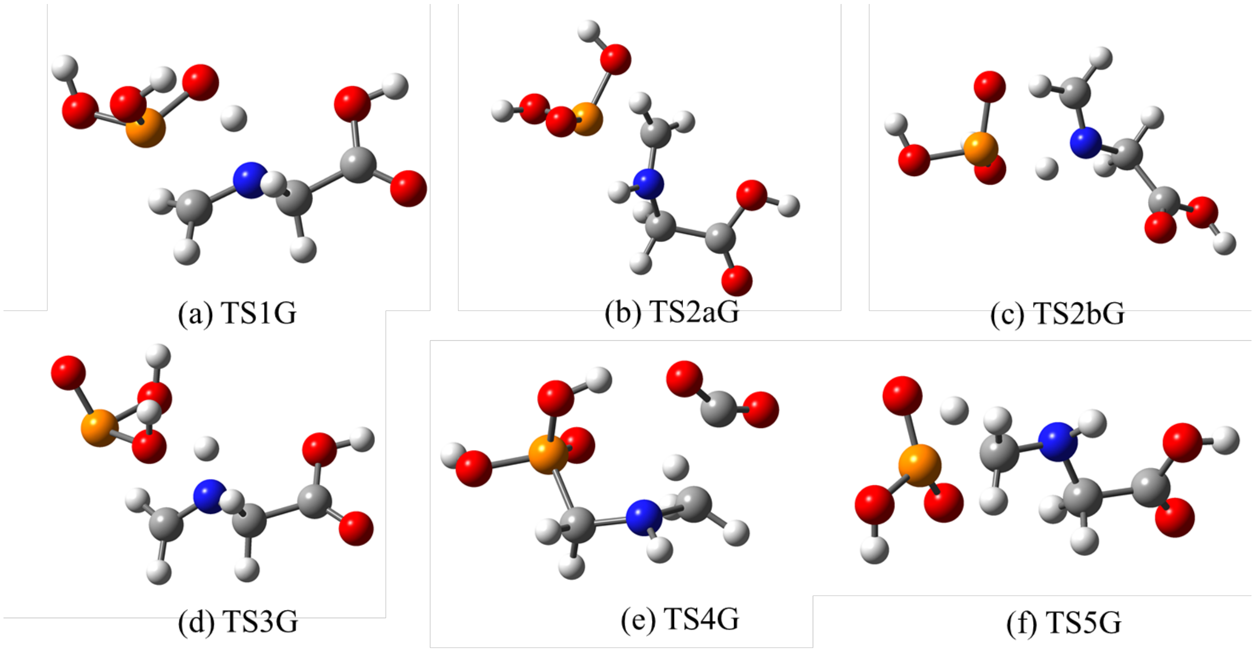
(a) TS1G
(b) TS2aG
(c) TS2bG
(d) TS3G
(e) TS4G
(f) TS5G

Fig. 3 Optimized structures for transition states identified in the thermal decomposition of GP. Transition state numbering is identified in Fig. 2.

The illustrated potential energy surface in Fig. 2 was used to calculated reaction rate coefficients (k) for GP thermal decomposition. For the two-step process of pathway 2, the first reaction was assumed to be the rate controlling step (i.e., leading directly to dissociated products). Rate coefficients across the temperature range 300 - 2000 K are shown in Fig. 4. The dominant reaction channel at all temperatures is the formation of $P(OH)_3$ and *N*-methylene-glycine via reaction channel 1. Rate coefficients for this process can be accurately expressed using the Arrhenius parameters $A = 9.12\times10^{13}$ s^{-1} and $E_a = 46.3$ kcal/mol.

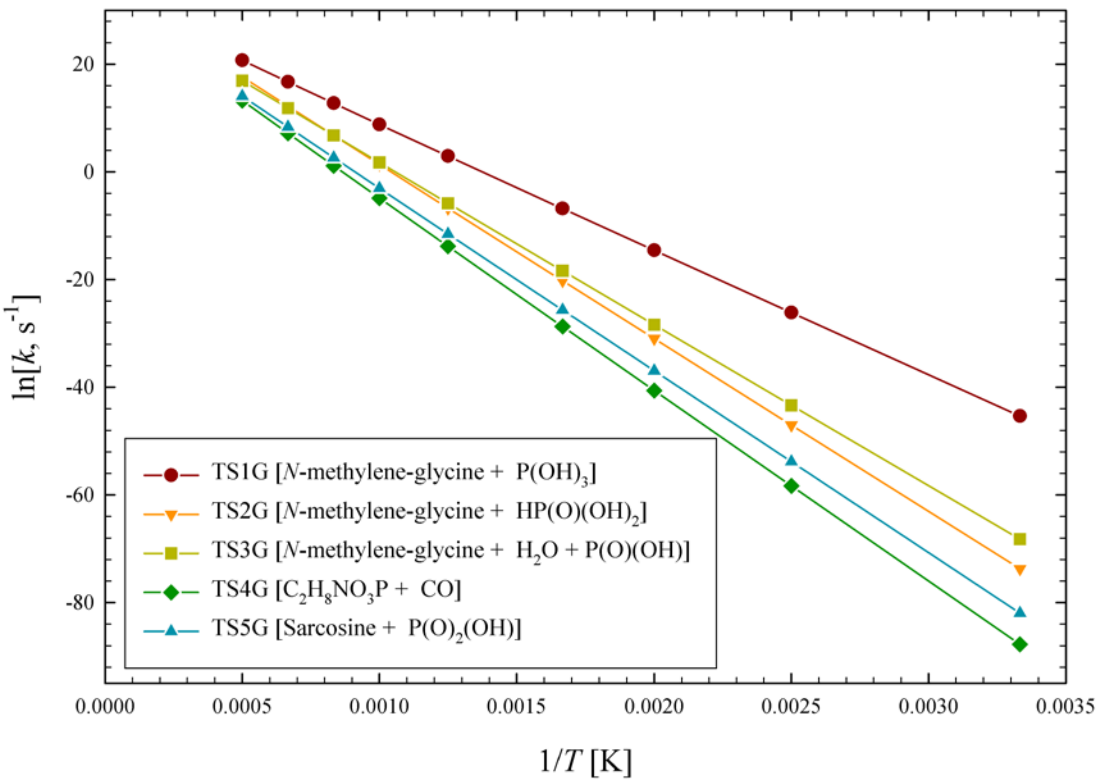

Fig. 4 Arrhenius plot of calculated GP thermal decomposition reaction rate coefficients, k (s^{-1}). Reaction pathways are identified in Fig. 2.

The calculated rate coefficients illustrated in Fig. 4, were used to evaluate branching ratios in GP decomposition. The branching ratio (k_i/k_t) is defined as the fraction of each reaction channel's rate coefficient (k_i) contributing to the overall rate coefficient (k_t). The branching ratio (in percentage) for all decomposition channels of GP from 300 to 2000 K are shown in Fig. 5. This graph demonstrates that reaction channel 1 dominates across the examined temperature range, where the share of other channels at 1200 K (for example) is less than 1%, and this is likely to be the only process required to model the first stage of GP decomposition.

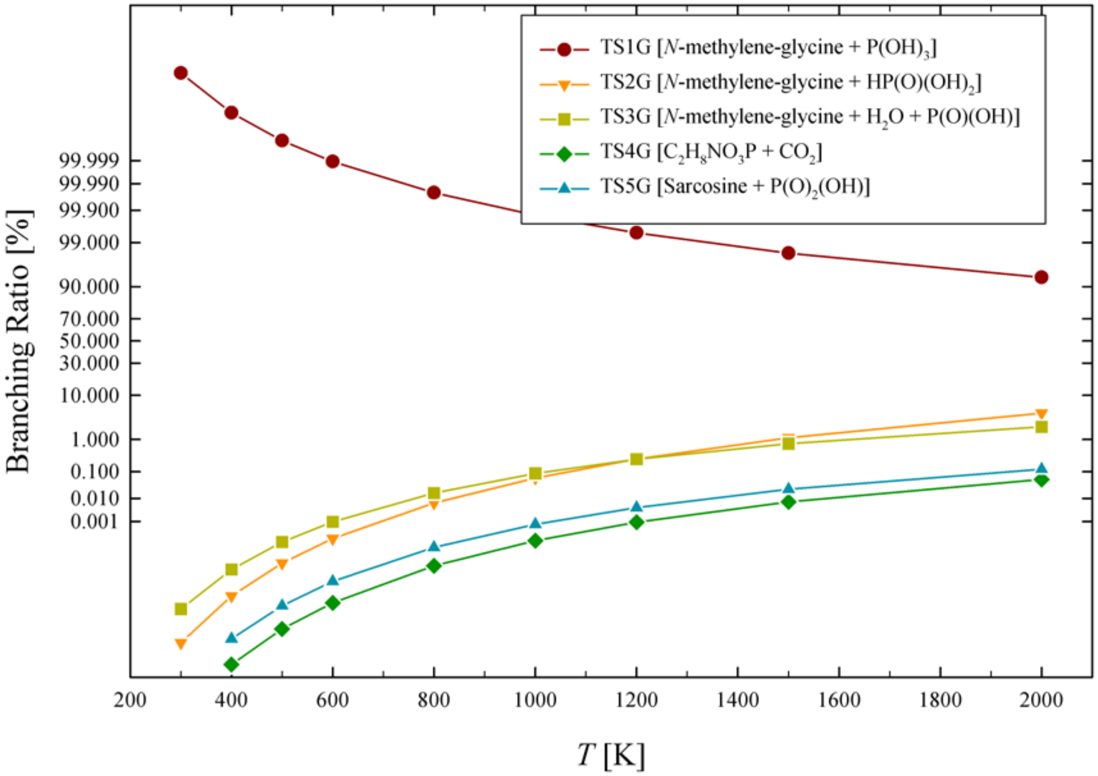

Fig. 5 Branching ratio (%) for each of the reaction channels identified in GP decomposition across the temperature range of 300 - 2000 K.

It is apparent that *N*-methylene-glycine will be the dominant decomposition product of GP, and we have therefore examined the further reaction chemistry of this important intermediate. A proposed decomposition mechanism for *N*-methylene-glycine involving decarboxylation is illustrated in Fig. 6a. In this reaction, the carboylate moiety donates a proton to the unsaturated CH_2=N group, in concert with CO_2 elimination, via **TS1MG**. This process leads to *N*-methyl methanimine and CO_2 with barrier height of 48.2 kcal/mol and reaction exothermicity of 9.2 kcal/mol. Given the similarity of barrier height to the first stage of GP decomposition, it is reasonable to expect that this would be relatively rapid at temperatures where GP forms *N*-methylene-glycine. This second step in the decomposition of GP is also qualitatively consistent with the experimental findings that the second stage of GP decomposition corresponds to an exothermic reaction with potential loss of the carbonyl (carboxylate) IR peak.[39] So as to incorporate this reaction process into kinetic model, rate coefficients have been calculated between 300 and 2000 K, resulting in the Arrhenius expression $k\ [\mathrm{s}^{-1}] = 1.63 \times 10^{12} e^{\frac{-48669}{RT}}$.

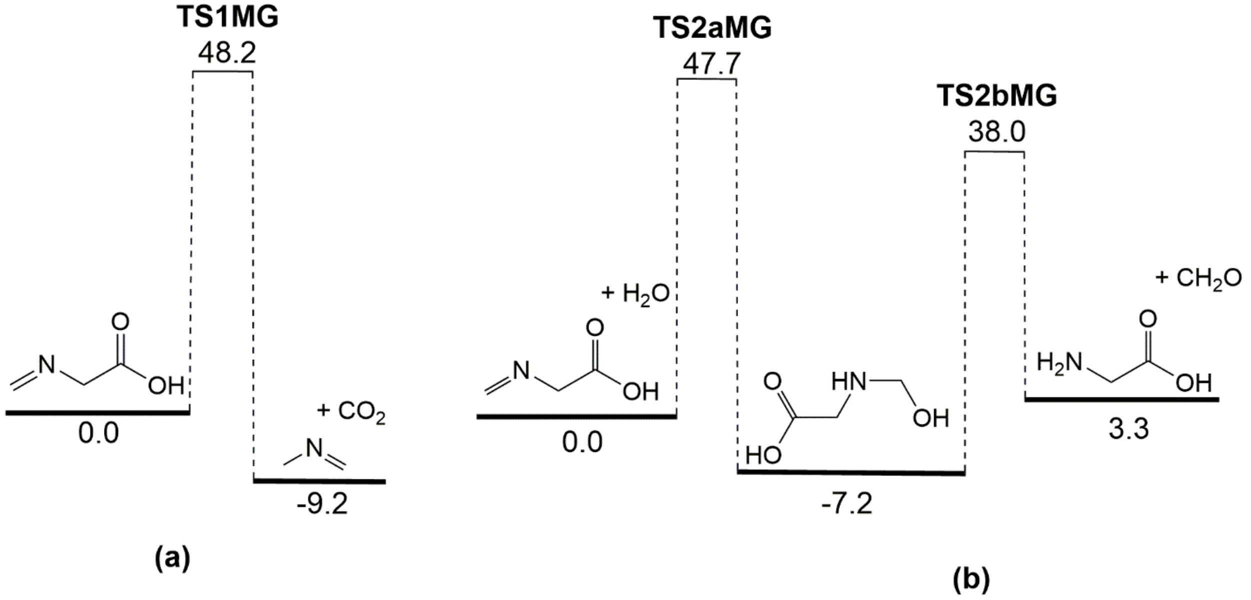

Fig. 6 Potential energy diagram for **(a)** *N*-methylene-glycine thermal decomposition, and **(b)** *N*-methylene-glycine hydrolysis. Energies (0 K enthalpies) are calculated at the G3X-K level of theory.

Imines are known to undergo hydrolysis reactions, and we therefore also investigated the competing bimolecular reaction of *N*-methylene-glycine with water. The potential energy surface for this reaction is shown in Fig. 6b, where it is seen to involve a two-step reaction pathway. The first step of this process involves proton transfer from water to the nitrogen atom, along with C—OH bond formation (**TS2aMG**). This is the rate-determining step, with barrier of 47.7 kcal/mol. Subsequent to this, proton transfer from the OH group to the nitrogen atom, along with N—C bond scission, transpires via **TS2bMG** with barrier of 38.0 kcal/mol relative to the reactants. Although this mechanism is comparable in energetics to that shown in Fig. 6a, the second order dependence on reagent concentrations means that it is unlikely to compete. However, in liquid water *N*-methylene-glycine may well follow this second decomposition pathway.

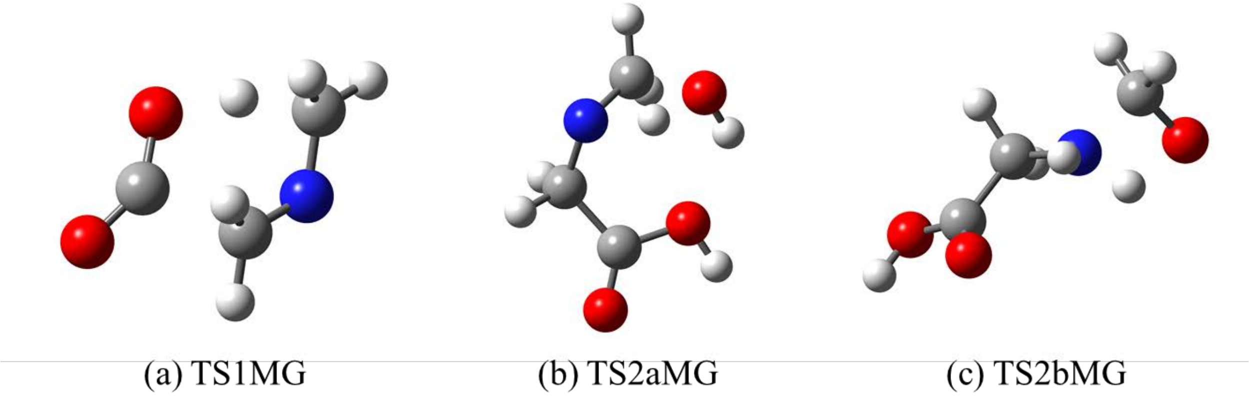
(a) TS1MG (b) TS2aMG (c) TS2bMG

Fig. 7 Optimized structures for transition states identified in (a) thermal decomposition, and (b-c) hydrolysis of *N*-methylene-glycine.

AMPA Decomposition

AMPA is the major metabolite of GP, and these two compounds are likely to co-exist in contaminated materials. Decomposition reaction channels identified for AMPA are illustrated in Fig. 6, where it can be concluded that the decomposition mechanism is very similar to that of GP. The reaction channel with the lowest barrier (50.1 kcal/mol) is again through $P(OH)_3$ elimination (**TS1A**) (Fig. 9a), where the final products are methanimine (CH_2NH) and $P(OH)_3$. Of the higher-energy reactions depicted in Fig. 8, two again lead to the same imine, $CH_2=NH$, either with $HP(O)(OH)_2$ (**TS2aA** and **TS2bA**) or HOPO + H_2O (**TS3A**). As with GP, amine formation can occur via loss of the phosphate group, with barrier height of 62.5 kcal/mol (**TS4A**).

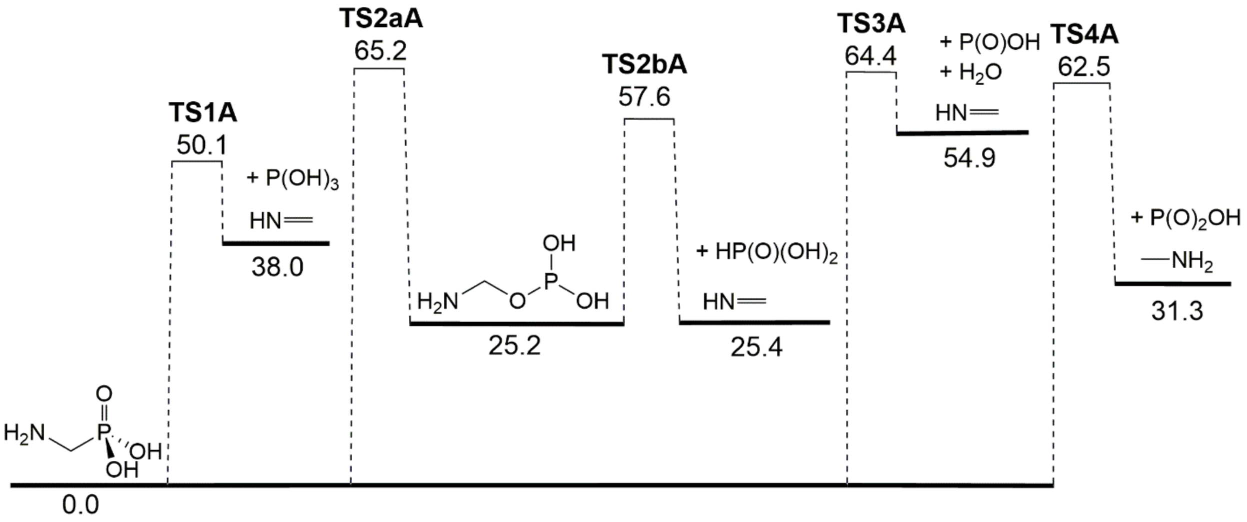

Fig. 8 Potential energy diagram for the thermal decomposition of AMPA. Energies (0 K enthalpies) are calculated at the G3X-K level of theory.

Of the higher-energy reactions depicted in Fig. 8, those closest to pathway 1 in energy again lead to the same imine, CH_2=NH, either with $HP(O)(OH)_2$ or HOPO + H_2O. As with GP, amine formation can occur via loss of the phosphate group.

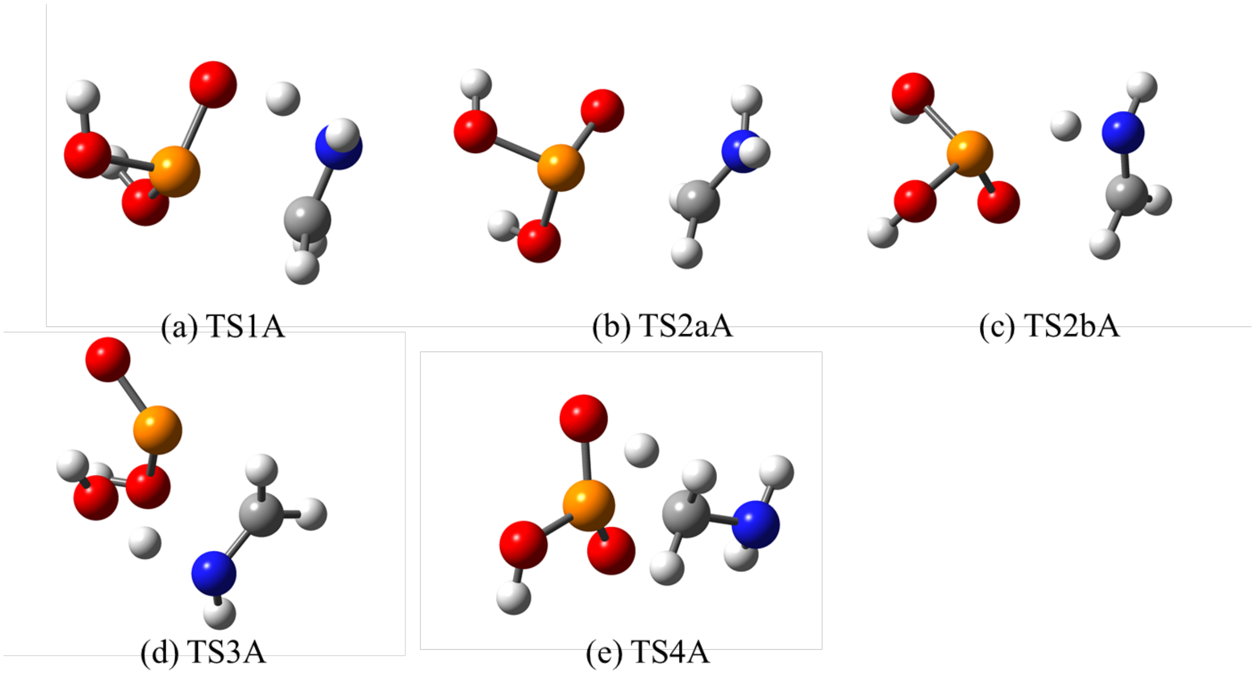
(a) TS1A (b) TS2aA (c) TS2bA (d) TS3A (e) TS4A

Fig. 9 Optimized structures for transition states identified in the thermal decomposition of AMPA. Transition state numbering is identified in Fig. 8.

The outlined potential surface energy for AMPA thermal decomposition was utilized to compute rate coefficients based on canonical transition state theory. The calculated rate coefficients for these five reaction channels over the temperature range 300 - 2000 K are shown in Fig. 10, and reaction channel 1 is kinetically dominant over all temperatures. Consequently, the compounds methanimine and phosphorous acid should be the main products of the first stage of AMPA decomposition. The Arrhenius parameters for this reaction over the applied temperature range are $A = 2.32\times10^{13}$ s^{-1} and $E_a = 50.9$ kcal/mol. Branching ratios are shown as Electronic Supplementary Information, and decomposition to methanimine and phosphorous acid is dominant across the entire temperature range. The reaction of methanimine with water in the gas phase has also been studied, where the mechanism is similar to that shown in Fig. 6b. This process will lead to ammonia and formaldehyde, and rate coefficients between 300 and 2000 K are described by the expression $k[\mathrm{cm}^3\mathrm{molecule}^{-1}\mathrm{s}^{-1}] = 5.77 \times 10^4 e^{\frac{-46817}{RT}}$.

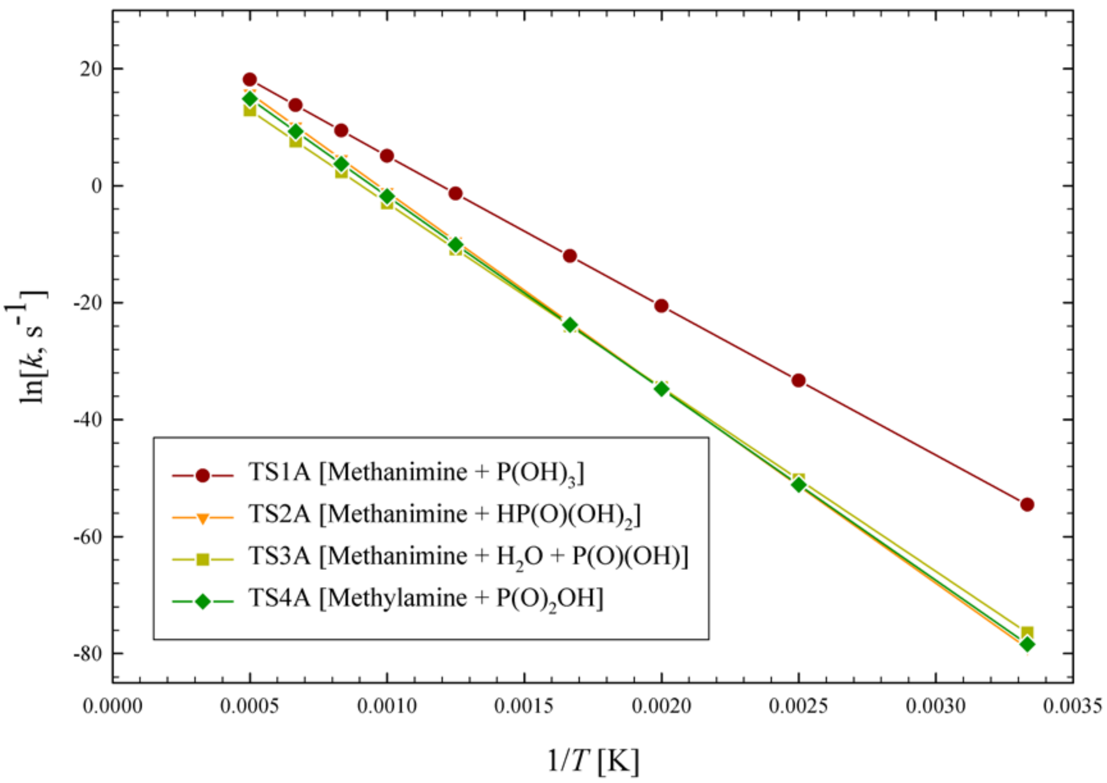

Fig. 10 Arrhenius plot of calculated AMPA thermal decomposition reaction rate coefficients, k (s^{-1}). Reaction pathways are identified in Fig. 8.

The half-life of dominant reaction channels for GP, *N*-methylene-glycine and AMPA decomposition are shown in Fig. 11. The half-life of GP is lower than its thermal decomposition intermediate, *N*-methylene-glycine, and metabolic product, AMPA. The half-life at 1000 K, which is a moderate temperature for conventional incineration processes, is below a millisecond for GP, and is several milliseconds for *N*-methylene-glycine and AMPA. These results reveal that the incineration or pyrolysis process can be applied for decomposition of GP waste in soil or wastewater with conversion to relatively benign products. Interestingly, AMPA has also been shown to have slower degradation kinetics than GP in catalytic destruction processes.[40]

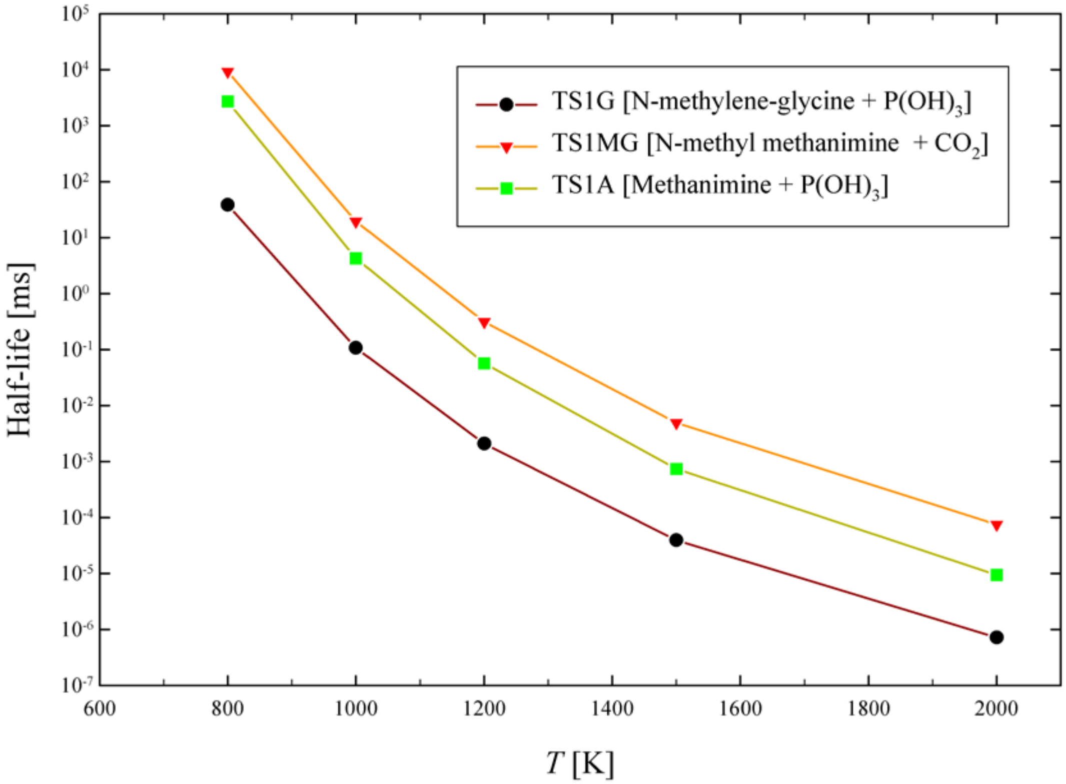

Fig. 11 Calculated half-life (ms) for thermal decomposition of GP, *N*-methylene-glycine and AMPA through their dominant reaction channels

In summary, GP and its metabolite AMPA can be thermally decomposed rapidly through the chemical mechanism newly reported here, as summarized in Scheme 1. Moreover, the thermolysis mechanism of GP reveals that its direct decomposition will not proceed through its toxic metabolite AMPA, instead forming *N*-methylene-glycine and then *N*-methyl-methanimine. Decomposition of AMPA directly produces methanimine. The imine products are expected to undergo hydrolysis reactions to ultimately produce relatively benign amines and aldehdyes. Importantly, none of these mechanisms proceed through free radical species, which may be environmentally persistent.[41, 42] These results will be helpful for developing incineration processes for the destruction of GP and AMPA, in addition to filling a gap in our fundamental understanding of their decomposition mechanisms.

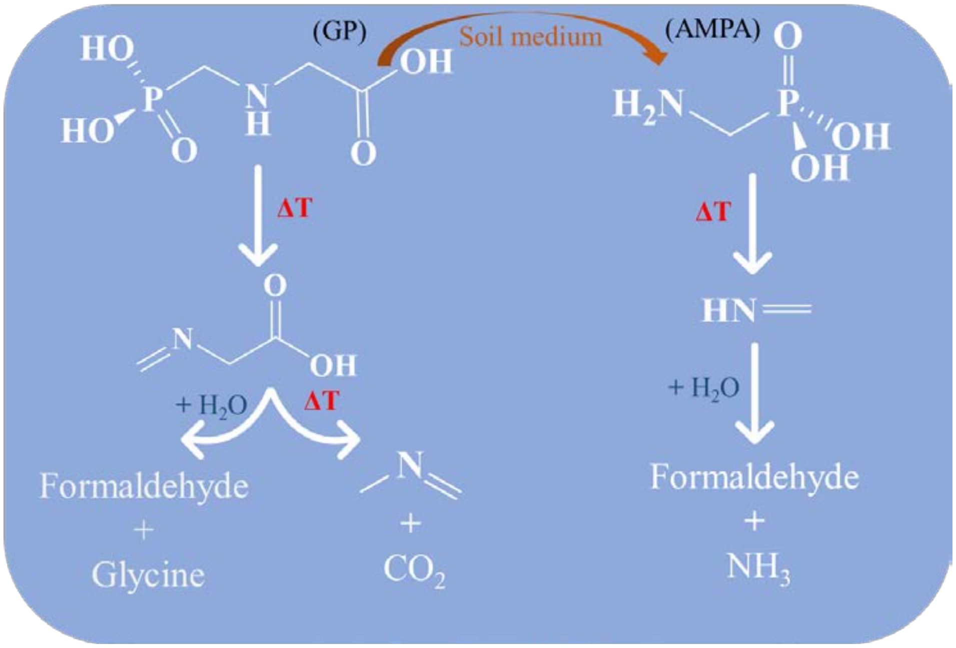

Scheme 1 Proposed thermal decomposition mechanism for glyphosate (GP) and aminomethylphosphonic acid (AMPA).

CONCLUSION

The thermochemical decomposition mechanism and kinetics of GP and AMPA have been examined by DFT and transition state theory calculations. Our findings reveal that the first stage of thermal decomposition of these organophosphorus compounds leads to elimination of phosphorous acid, with the co-product being *N*-methylene-glycine (for GP) or methanimine (for AMPA). Calculated rate coefficients from 300 – 2000 K confirm the dominant contribution of these pathways over other competing processes. The second stage of GP pyrolysis is shown to involve *N*-methylene-glycine decomposition to *N*-methyl-methanimine + CO_2, whereas for AMPA the primary decomposition product methanimine is expected to react with water to yield formaldehyde and ammonia. These results can help to gain a better understanding of the fate of these organic phosphoric substances in thermal processes and to design and improve facilities efficiency for their destruction.

Electronic Supplementary Information Available: Calculated rate coefficients and branching ratios; potential energy diagram for methanimine hydrolysis; relative energies, moments of inertia, vibrational frequencies, and Cartesian coordinates of all species.

Conflicts of interest

There are no conflicts to declare.

Acknowledgements

This work was supported through the Australian Research Council Future Fellowships scheme, FT130101304.

References

1. A. D. Baylis, Why glyphosate is a global herbicide: strengths, weaknesses and prospects, *Pest Manage. Sci.*, 2000, **56**, 299-308.
2. A. T. Woodburn, Glyphosate: production, pricing and use worldwide, *Pest Manage. Sci.*, 2000, **56**, 309-312.
3. S. O. Duke and S. B. Powles, Glyphosate: a once-in-a-century herbicide, *Pest Manage. Sci.*, 2008, **64**, 319-325.
4. D. R. Van Stempvoort, J. Spoelstra, N. D. Senger, S. J. Brown, R. Post and J. Struger, Glyphosate residues in rural groundwater, Nottawasaga River watershed, Ontario, Canada, *Pest Manage. Sci.*, 2016, **72**, 1862-1872.
5. H. Li, A. F. Wallace, M. Sun, P. Reardon and D. P. Jaisi, Degradation of glyphosate by Mn-oxide may bypass sarcosine and form glycine directly after C–N bond cleavage, *Environ. Sci. Technol.*, 2018, **52**, 1109-1117.
6. A. J. L. Catão and A. López-Castillo, On the degradation pathway of glyphosate and glycine, *Environ. Sci.: Processes Impacts*, 2018, **20**, 1148-1157.

7. A. Gosset, C. Durrieu, F. Orias, R. Bayard and Y. Perrodin, Identification and assessment of ecotoxicological hazards attributable to pollutants in urban wet weather discharges, *Environ. Sci.: Processes Impacts*, 2017, **19**, 1150-1168.
8. T. Poiger, I. J. Buerge, A. Bächli, M. D. Müller and M. E. Balmer, Occurrence of the herbicide glyphosate and its metabolite AMPA in surface waters in Switzerland determined with on-line solid phase extraction LC-MS/MS, *Environ. Sci. Pollut. Res.*, 2017, **24**, 1588-1596.
9. M. P. Gomes, E. Smedbol, A. Chalifour, L. Hénault-Ethier, M. Labrecque, L. Lepage, M. Lucotte and P. Juneau, Alteration of plant physiology by glyphosate and its by-product aminomethylphosphonic acid: an overview, *J. Exp. Bot.*, 2014, **65**, 4691-4703.
10. A. J. Al-Rajab and M. Schiavon, Degradation of 14C-glyphosate and aminomethylphosphonic acid (AMPA) in three agricultural soils, *J. Environ. Sci.*, 2010, **22**, 1374-1380.
11. B. Singh and K. Singh, Microbial degradation of herbicides, *Crit. Rev. Microbiol.*, 2016, **42**, 245-261.
12. D. P. Jaisi, H. Li, A. F. Wallace, P. Paudel, M. Sun, A. Balakrishna and R. N. Lerch, Mechanisms of bond cleavage during manganese oxide and UV degradation of glyphosate: results from phosphate oxygen isotopes and molecular simulations, *J. Agric. Food Chem.*, 2016, **64**, 8474-8482.
13. D. W. Kolpin, E. M. Thurman, E. A. Lee, M. T. Meyer, E. T. Furlong and S. T. Glassmeyer, Urban contributions of glyphosate and its degradate AMPA to streams in the United States, *Sci. Total Environ.*, 2006, **354**, 191-197.
14. C. Skark, N. Zullei-Seibert, U. Schöttler and C. Schlett, The occurrence of glyphosate in surface water, *Int. J. Environ. Anal. Chem.*, 1998, **70**, 93-104.
15. N. Lin and V. Garry, In vitro studies of cellular and molecular developmental toxicity of adjuvants, herbicides, and fungicides commonly used in Red River Valley, Minnesota, *J. Toxicol. Environ. Health, Part A*, 2000, **60**, 423-439.
16. F. Mañas, L. Peralta, J. Raviolo, H. G. Ovando, A. Weyers, L. Ugnia, M. G. Cid, I. Larripa and N. Gorla, Genotoxicity of glyphosate assessed by the comet assay and cytogenetic tests, *Environ. Toxicol. Pharmacol.*, 2009, **28**, 37-41.
17. C. Gasnier, C. Dumont, N. Benachour, E. Clair, M.-C. Chagnon and G.-E. Séralini, Glyphosate-based herbicides are toxic and endocrine disruptors in human cell lines, *Toxicology*, 2009, **262**, 184-191.
18. S. H. Bai and S. M. Ogbourne, Glyphosate: environmental contamination, toxicity and potential risks to human health via food contamination, *Environ. Sci. Pollut. Res.*, 2016, **23**, 18988-19001.
19. M. Rodrigo, N. Oturan and M. A. Oturan, Electrochemically assisted remediation of pesticides in soils and water: a review, *Chem. Rev. (Washington, DC, U. S.)*, 2014, **114**, 8720-8745.
20. Z. Ren, Y. Dong and Y. Liu, Enhanced glyphosate removal by montmorillonite in the presence of Fe (III), *Ind. Eng. Chem. Res.*, 2014, **53**, 14485-14492.
21. M. Mohsen Nourouzi, T. Chuah and T. S. Choong, Adsorption of glyphosate onto activated carbon derived from waste newspaper, *Desalin. Water Treat.*, 2010, **24**, 321-326.
22. T. F. Speth, Glyphosate removal from drinking water, *J. Environ. Sci.*, 1993, **119**, 1139-1157.
23. J. Song, X.-M. Li, A. Figoli, H. Huang, C. Pan, T. He and B. Jiang, Composite hollow fiber nanofiltration membranes for recovery of glyphosate from saline wastewater, *Water Res.*, 2013, **47**, 2065-2074.
24. M. D. Zhang, Y. F. Wei, K. Zhao, R. W. Mei and M. Huang, presented in part at the Advanced Materials Research, 2011.
25. L. Cao, D. Ma, Z. Zhou, C. Xu, C. Cao, P. Zhao and Q. Huang, Efficient photocatalytic degradation of herbicide glyphosate in water by magnetically separable and recyclable BiOBr/Fe3O4 nanocomposites under visible light irradiation, *Chem. Eng. J.* , 2019, **368**, 212-222.
26. K. Barrett and M. McBride, Oxidative degradation of glyphosate and aminomethylphosphonate by manganese oxide, *Environ. Sci. Technol.*, 2005, **39**, 9223-9228.
27. A. Manassero, C. Passalia, A. C. Negro, A. E. Cassano and C. S. Zalazar, Glyphosate degradation in water employing the H2O2/UVC process, *Water Res.*, 2010, **44**, 3875-3882.

28. P. A. Vesilind and T. B. Ramsey, Effect of drying temperature on the fuel value of wastewater sludge, *Waste Manage. Res.*, 1996, **14**, 189-196.
29. E. Zegers and E. Fisher, Gas-phase pyrolysis of diethyl methylphosphonate, *Combust. Sci. Technol.*, 1996, **116**, 69-89.
30. E. Zegers and E. Fisher, Gas-phase pyrolysis of diisopropyl methylphosphonate, *Combust. Flame*, 1998, **115**, 230-240.
31. P. Glaude, H. Curran, W. Pitz and C. Westbrook, Kinetic study of the combustion of organophosphorus compounds, *Proc. Combust. Inst.*, 2000, **28**, 1749-1756.
32. P. Glaude, C. Melius, W. Pitz and C. Westbrook, Detailed chemical kinetic reaction mechanisms for incineration of organophosphorus and fluoroorganophosphorus compounds, *Proc. Combust. Inst.*, 2002, **29**, 2469-2476.
33. J. H. Werner and T. A. Cool, Kinetic model for the decomposition of DMMP in a hydrogen/oxygen flame, *Combust. Flame*, 1999, **117**, 78-98.
34. M. F. M. Nogueira and E. Fisher, Effects of dimethyl methylphosphonate on premixed methane flames, *Combust. Flame*, 2003, **132**, 352-363.
35. M. Frisch, G. Trucks, H. Schlegel, G. Scuseria, M. Robb, J. Cheeseman, G. Scalmani, V. Barone, G. Petersson and H. Nakatsuji, Gaussian 16 (Revision A), Gaussian Inc., Pittsburgh, PA, 2016.
36. G. da Silva, G3X-K theory: A composite theoretical method for thermochemical kinetics, *Chem. Phys. Lett.*, 2013, **558**, 109-113.
37. J. Barker, T. Nguyen, J. Stanton, C. Aieta, M. Ceotto, F. Gabas, T. Kumar, C. Li, L. Lohr and A. Maranzana, MultiWell-2016 Software Suite, JR Barker, University of Michigan, 2016.
38. J. R. Barker, Multiple-Well, multiple-path unimolecular reaction systems. I. MultiWell computer program suite, *Int. J. Chem. Kinet.*, 2001, **33**, 232-245.
39. F.-X. Chen, C.-R. Zhou and G.-P. Li, Study on thermal decomposition and the non-isothermal decomposition kinetics of glyphosate, *J. Therm. Anal. Calorim.*, 2012, **109**, 1457-1462.
40. H. Li, S. R. Joshi and D. P. Jaisi, Degradation and isotope source tracking of glyphosate and aminomethylphosphonic acid, *J. Agric. Food Chem.*, 2016, **64**, 529-538.
41. B. Dellinger, S. Lomnicki, L. Khachatryan, Z. Maskos, R. W. Hall, J. Adounkpe, C. McFerrin and H. Truong, Formation and stabilization of persistent free radicals, *Proc. Combust. Inst.*, 2007, **31**, 521-528.
42. E. P. Vejerano, G. Rao, L. Khachatryan, S. A. Cormier and S. Lomnicki, Environmentally persistent free radicals: insights on a new class of pollutants, *Environ. Sci. Technol.*, 2018, **52**, 2468-2481.